

Chapter 14

Microstructure and Properties of the Fusion Zone in Steel-Cast Iron Composite Castings



Lukas Apfelbacher, Patrick Hegele, Arne Davids, Leonhard Hitzler,
Christian Kremaszky, and Ewald Werner

Abstract Casting is an established way to manufacture metal components with complex geometry and high wall thickness at low cost. However, the possibilities for locally modifying material properties are limited in conventional casting processes. These limitations can be remedied by utilizing composite casting. Within this study, a lamellar graphite cast iron melt was poured into low carbon steel shells comprised the steels S235JR and 25CrMo4, differing in their mechanical properties and their thermal conductivity, with the aim to form a material bond. Three different temperatures for the steel shells at the time of pouring were investigated: 293, 383 and 583 K. After preheating, the shells were embedded in unheated sand moulds, which were then filled with an EN-GJL-250 melt. The resulting fusion zone was characterized using optical microscopy, and the mechanical properties were assessed by Brinell hardness tests. The properties and microstructural morphology around the fusion zone strongly depend on the initial temperature of the shell at the time of casting. For shell temperatures of 293 K, no proper bonding was achieved between shell and core. A pearlite layer with a thickness of up to 500 μm was formed at a temperature of 583 K, whilst the adjacent region of the cast iron became decarburized. The hardness of the fusion zone reached a maximum of 275 HBW for a shell temperature of 383 K with an overall span from 235 to 275 HBW.

L. Apfelbacher (✉) · P. Hegele · A. Davids · L. Hitzler · C. Kremaszky · E. Werner
School of Engineering and Design, Institute of Materials Science and Mechanics of Materials,
Technical University of Munich, 85748 Garching, Germany
e-mail: l.apfelbacher@tum.de

P. Hegele
e-mail: patrick.hegele@tum.de

A. Davids
e-mail: arne.davids@tum.de

L. Hitzler
e-mail: Leonhard.hitzler@tum.de

C. Kremaszky
e-mail: kremaszky@tum.de

E. Werner
e-mail: ewald.werner@tum.de

Keywords Composite casting · Compound casting · Grey cast iron · Fusion zone · Material-fit connection

14.1 Introduction

Joining two different materials in one part to locally combine and tailor different properties can be achieved either by a form-fit, a force-fit or a material-fit connection mechanism (Khrebtov 2011; DIN 8593:2003). Form-fit connections include, for example, bolted and riveted connections. Crimped connections are an example of a force-fit connection. Material-fit connections *inter alia* include adhesive or welded joints (Moro 2022; DIN 8593:2003). A solid bond can be achieved via all three aforementioned mechanisms, each with its specific advantages and disadvantages.

All these mechanisms can be exploited in joining metallic constituents by composite casting (Noguchi 2008). This process is characterized by casting melt onto an insert or into a mould, which at least partially becomes the final component itself. In doing so, a form-fit connection is achieved when the solidified melt interlocks with serrations in the insert or the shell. This is the dominant joining mechanism in high pressure die casting (HPDC), where steel inserts are recast with an aluminium melt to increase the mechanical properties of the composite (Elliott 1988, Schittenhelm 2018). Furthermore, differences in the thermal expansion coefficients (CTE) of composite casting constituents can be utilized for joining by the force-fit mechanism. An industrially established example based on this principle is the connection of steel tubes with cast aluminium joints for automotive applications (Dörr and Wibbeke 2008). Finally, a connection in composite casting can also be established by a material fit. A typical process employing this mechanism exhibits a bond formation in three mostly simultaneous stages: (i) partial fusing of the metallic inserts due to the thermal capacity of the added melt, (ii) mixing of the atomic constituents mainly amongst the involved liquids by interdiffusion and convection, and (iii) adherent solidification onto the residuals of the inserts by heterogeneous nucleation or grain growth. The resulting connections are microstructurally smooth and, hence, exhibit a gradual transition in macroscopic properties (e.g. in Young's modulus, CTE or chemical potential).

This is expected to be advantageous in comparison with sharp transitions created by the aforementioned composite casting approaches concerning mechanical and thermal load-bearing capabilities as well as in corrosive environments. Furthermore, material-fit composite casting enables new design possibilities—regarding the material thickness and accessibility of bonds—not feasible within related conventional joining technologies like welding.

Nevertheless, similar to welding processes, design limitations for material-fit composite casting have to be considered. For example, excessively thin metal shells bear the risk of softening during the process leading to leakage of melt. This risk increases, if the superheating of the melt becomes higher in comparison with the melting point of the shell. Ideally, just a marginal but sufficient amount of the shell is

fused to form a dense alloy layer without unnecessarily affecting its overall properties. Moreover, it is evident that chemically similar materials are more suited for composite casting with the aim for a material-fit bond, due to the fact that the remelting of the shell required for fusion is more likely to happen without the need for extensive pre-treatment (Ibleib et al. 1995).

Despite considering these limitations, the formation of a reproducible and distinct transition zone and, hence, a reliable material bond is not necessarily given (Buchmayr and Weligoschek 2010; Krause 1990). For example, in conventional sand casting metallic inserts, called chills, are used to control the solidification of the cast. They increase heat dissipation locally without forming a proper bond with the cast material and can be removed after casting (Jaromin et al. 2019). Therefore, a series of pre-treatment steps is commonly applied to achieve a bonding and to overcome differences in the thermo-physical properties. Viable results have been achieved with metallic coatings (Bakke et al. 2022). However, coating of the shells can be tedious and costly. A new approach is based on preheating the shells.

To study this processing route in detail, the effect of three different shell temperatures at the time of pouring on the bond formation between low carbon steel shells and a lamellar grey iron cast was investigated in this work.

Fe-based alloys were selected for both joining partners to enhance the probability to form a sufficient bond. Nevertheless, these material classes are quite different in their material properties. On the one hand, low carbon steels can be formed easily to thin wall thickness to become the casting mould whilst retaining sufficient structural strength during casting. On the other hand, lamellar grey iron offers increased thermal conductivity and vibration damping but suffers from significantly lower mechanical properties. The combination of the two material classes offers the possibility to achieve better thermo-physical properties, compared to a single-material part, which can be even further tuned by a tailored selection of alloys within the specific material classes. To investigate the influence of this fine-tuning on the transition zone, examinations were applied to shells comprised two distinct low carbon steels.

14.2 Experimental Details

14.2.1 Composite Casting

The grey iron EN-GJL-250 (DIN EN 1561:2012-01) was obtained from recycled material. The thickness ratio of melt to steel was 20:1, with a wall thickness of the steel shells of 5 mm. One shell was made of a S235JR alloy and the second one of 25CrMo4 with a thermal conductivity of 40 W/mK and 49 W/mK, respectively (Gruppo Lucefin 2012; DEW 2011). In Table 14.1, the chemical composition of the employed materials, determined via optical emission spectroscopy (Spectromaxx-LMX06, SPECTRO Analytical Instruments GmbH), is provided.

Table 14.1 Chemical composition of shell and cast materials in wt.%

Material	C	Si	Mn	Mo	Cu	Cr	Ni	Ti	Fe
EN-GJL-250	3.44	1.94	0.64	0.03	0.24	0.16	–	0.16	Balance
S235JR	0.08	0.01	0.52	0.01	0.02	0.01	0.01	–	Balance
25CrMo4	0.24	0.23	0.61	0.18	0.21	0.96	0.19	–	Balance

The steel shells were pre-treated by shot blasting with alumina (0.25–0.5 mm). Preheating was conducted in a Nabertherm L3/11 electrical resistance furnace in air (Nabertherm GmbH). Three shell temperatures T_{shell} were targeted at the time of the pouring: 293, 383 and 583 K. To accomplish these, the steel shells were superheated approximately 50 K above the desired T_{shell} in a furnace. Then, the superheated steel shells were placed without delay into the copes of the two-part casting flasks, which themselves were not preheated to reflect industrial production conditions. After the targeted shell temperature, which was measured with K-type thermocouples brazed to the shells, was reached, the moulds were filled with the grey cast iron melt. For inoculation 0.15 wt.% FeSi (Elkem SuperSeed 75, Elkem ASA, Norway) was placed in the sprue. This step, in addition to the increased Si content of the cast iron, was taken to avoid metastable carbide formation (chill) and secure grey solidification. The resulting microstructure is expected to be fully pearlitic with graphite lamellae. Figure 14.1 shows a schematic sketch of an assembled flask, including the embedded steel shell. The melt was poured into the cup to ensure a rising cast.

Table 14.2 outlines the shell materials and the targeted temperatures T_{shell} of these inserts at the time of pouring for the samples. The temperature of the melt at pouring was 1673 K for all samples produced.

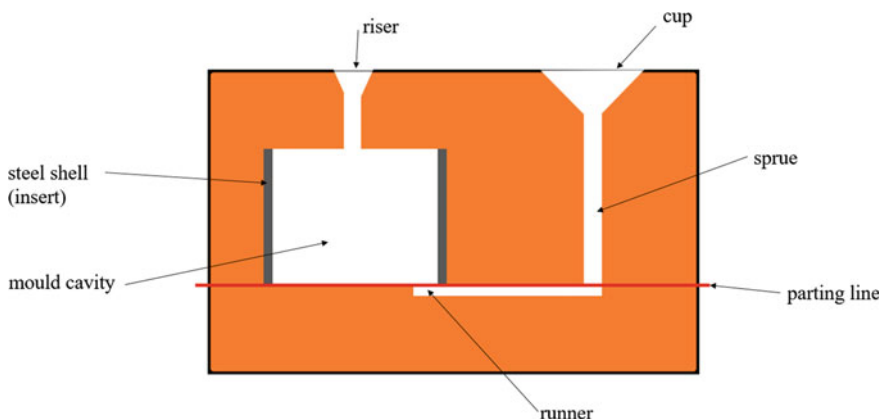


Fig. 14.1 Schematic sketch of the flask, consisting of the heated steel shell embedded in the unheated green sand mould

Table 14.2 Configurations of the fabricated samples, material combination and shell temperature

Sample	1	2	3	4	5	6
Shell	S235JR	25CrMo4	S235JR	25CrMo4	S235JR	25CrMo4
T_{shell} (K)	293	293	383	383	583	583

Table 14.3 Preparation steps for metallographic sections

Disc	Abrasive	Lubricant	rpm	Force (N)	Time (min)
SiC 220	–	Water	300	180	Till plane
MD Allegro	9 μm	DP lubricant blue	150	180	4
MD-Dac	3 μm	DP lubricant blue	150	180	4
MD-Mol	1 μm	–	150	120	6

14.2.2 Microstructure Observation

A metallographic preparation was applied to sections of the samples that were within a plane perpendicular to the outer surface of the shell and located around the fusion zone and half of the mould in filling direction. The preparation is detailed in Table 14.3. A light optical microscope Axio Scope.A1 (Zeiss) was used for image acquisition. The graphite structure was analysed according to EN ISO 945-1:2019, and, after etching with 3% alcoholic nitric acid (Nital), the microstructure was evaluated according to DIN 50600:2017-10.

14.2.3 Hardness Measurement

The measurement of Brinell hardness (HBW 5/750) was performed according to EN ISO 6506-1:2014, utilizing a Dia Testor 2Rc (Otto Wolpert-Werke). Measurements were taken from three different areas, namely the cast iron core, the fusion zone and the steel shell. Ten hardness indentations distributed over the entire height of the samples for each of the three microstructural zones were evaluated.

14.3 Results

14.3.1 Graphite Morphology

The graphite morphology was assessed in accordance with DIN EN ISO 945-1:2019. The graphite forms present are depicted in Fig. 14.2, whilst Fig. 14.3 shows the different arrangements of graphite lamellae. Figures 14.4 and 14.5 show the graphite

Fig. 14.2 Graphite forms IV (left) and V (right). Excerpt from: directional series diagrams for main forms of graphite in cast iron according to DIN EN ISO 945-1:2019

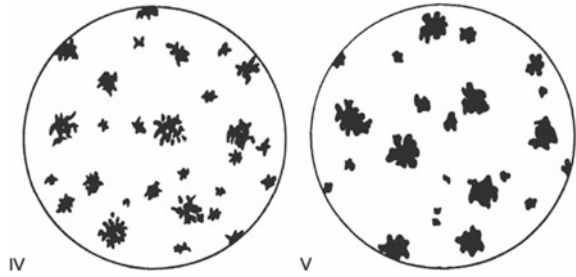


Fig. 14.3 Graphite arrangements A (left), D (middle) and E (right). Excerpt from: directional series diagrams for arrangement of graphite in cast iron according to DIN EN ISO 945-1:2019

morphology of the composite samples. For the unheated shell, no continuous bonding between the steel shell and the cast iron core was achieved. Spherical graphite precipitates were evident in the dendritic microstructure of the cast iron core. These irregular graphite spheres could be assigned to the graphite forms IV and V (Figs. 14.4a and 14.5a). In addition, small areas with D-graphite (interdendritic graphite with random orientation) were present. After pouring the melt into the shell preheated to 383 K, nearly only D-graphite was present in the fusion zone (Figs. 14.4b and 14.5b). Graphite lamellae of arrangement A only occurred isolated for sample 3 (Fig. 14.4b) and in a few areas in sample 4, near the bonding line (Fig. 14.5b). A shell temperature of 583 K led to the graphite morphology typical for EN-GJL-250, consisting of long lamellae of type A- and E-graphite (Figs. 14.4c and 14.5c).

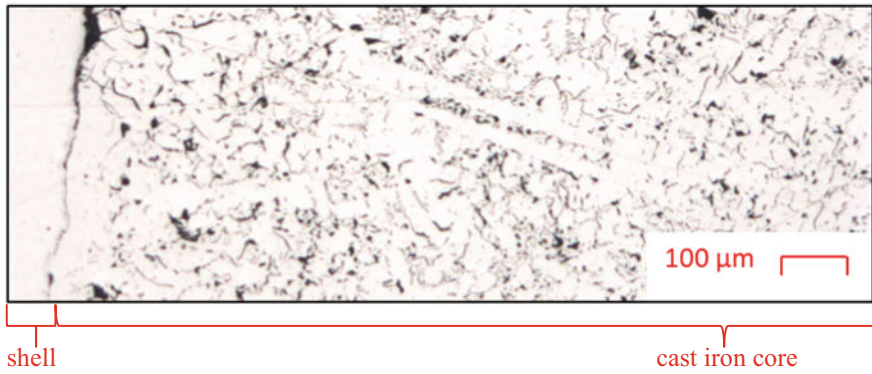
14.3.2 Etched Microstructure

Figures 14.6 and 14.7 show the microstructure after etching. For samples cast at a shell temperature of 293 K, no fusion zone was evident, irrespective of the shell material used. The cast iron contained some ferritic structures in the region adjacent to the fusion zone for both shell materials (Figs. 14.6a and 14.7a). These structures were significantly more pronounced in the 25CrMo4 sample, where local ferrite seams formed near the gap between the two materials. In the same area, the steel

(a) Sample 1 (S235JR, 293 K)



(b) Sample 3 (S235JR, 383 K)



(c) Sample 5 (S235JR, 583 K)

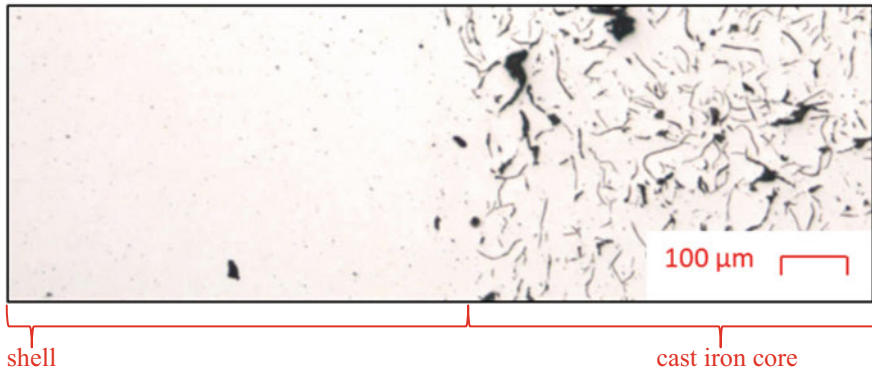
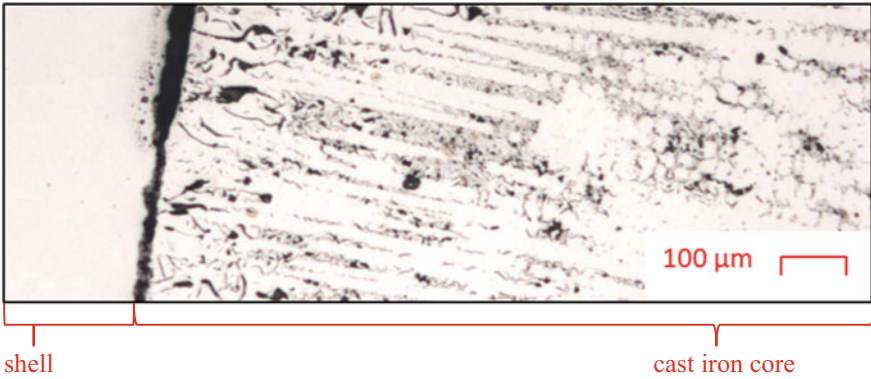
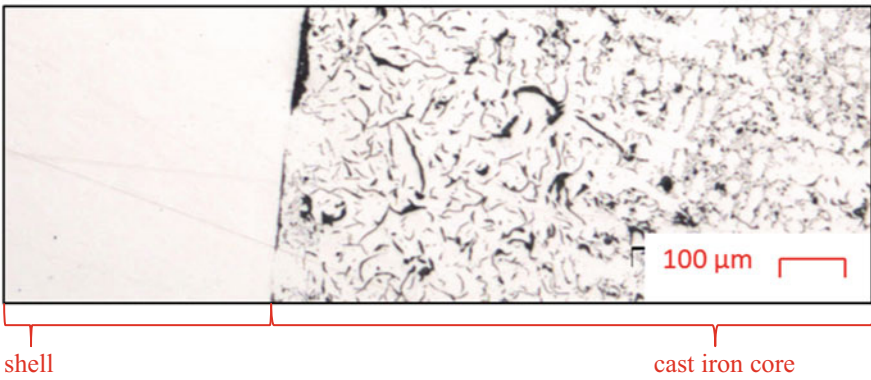


Fig. 14.4 Micrographs of the composite samples with nomenclature according to Table 14.2, showing the graphite morphology in the fusion zone for the shell temperatures at the time of the pouring. **a** 293 K, **b** 383 K, **c** 583 K. The shell material S235JR is seen on the left, the EN-GJL-250 cast iron core on the right

a) Sample 2 (25CrMo4, 293 K)



b) Sample 4 (25CrMo4, 383 K)



c) Sample 6 (25CrMo4, 583 K)

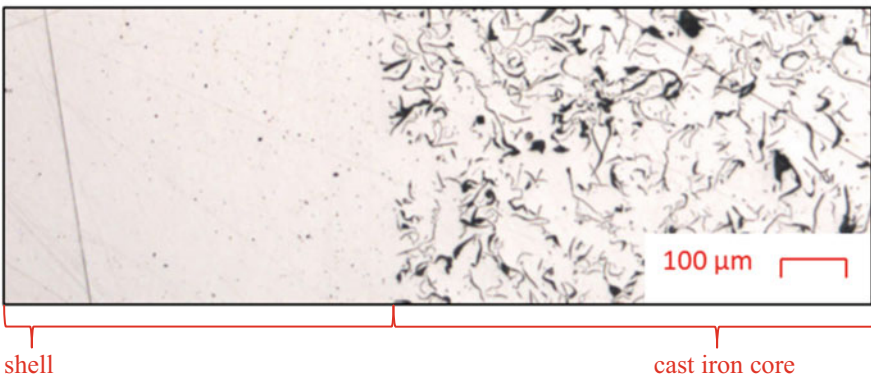


Fig. 14.5 Micrographs of the composite samples with nomenclature according to Table 14.2, showing the graphite morphology in the fusion zone for the shell temperatures at the time of the pouring. **a** 293 K, **b** 383 K, **c** 583 K. The shell material 25CrMo4 is seen on the left, the EN-GJL-250 cast iron core on the right

shell also becomes decarburized (Fig. 14.7a). A shell temperature of 383 K led to the formation of a bonding layer over large parts of the samples, whereby a pearlitisation of approximately 300 μm into the steel shell was noted (Figs. 14.6b and 14.7b). The microstructure of the cast iron core consisted of pearlite. A shell temperature of 583 K led to a completely pearlitic cast microstructure in the examined area near the fusion zone. In addition, the steel shell underwent a pearlitic transformation. The transformed zone had a thickness of approximately 500 μm . For both shell materials, a coarsening of the grains in the steel could be observed at 583 K in comparison with the lower shell temperatures (Figs. 14.6c and 14.7c).

14.3.3 Hardness

The hardness of the samples with a S235JR shell is shown in Fig. 14.8a. The hardness of the cast iron ranged between 190 and 235 HBW, which are typical values for EN-GJL-250¹ (DIN EN 1561:2012-01). The hardness of the shell material was 120 HBW. This is in agreement with the technical data sheet provided by the supplier (Gruppo Lucefin 2012). At a shell temperature of 293 K, no bonding between the shell and the cast iron could be achieved. Therefore, no hardness could be determined for the fusion zone in these instances. A shell temperature of 383 K resulted in a fusion zone with hardness values between 235 and 295 HBW. For a shell temperature of 583 K, the hardness of the fusion zone ranged between 250 and 260 HBW, which was only slightly above the hardness of the cast iron core. Figure 14.8b shows the hardness values for the sample with the 25CrMo4 shell. The hardness values for the cast iron core and the fusion zone were similar to those of the S235JR shell sample in Fig. 14.8a. The hardness of the 25CrMo4 steel shell was 210 HBW, which is in agreement with the technical data sheet provided by the supplier (DEW Witten 2011).

14.4 Discussion

In this study, the influence of the chemical composition of the shell and the shell temperature at the time of the pouring T_{shell} on the resulting fusion zone were investigated.

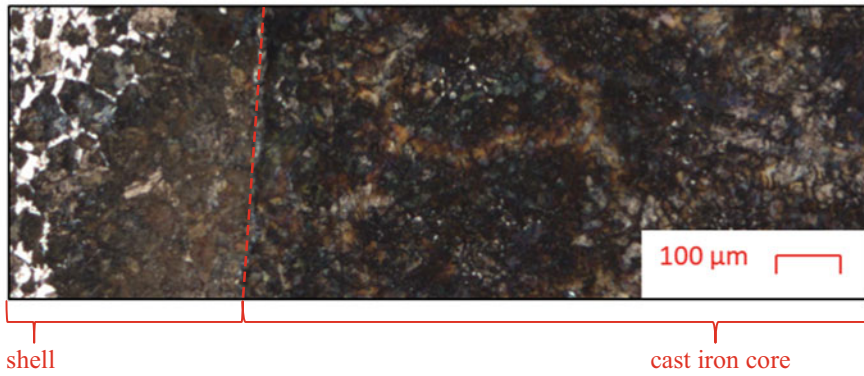
The microstructure of the samples was significantly influenced by the initial temperature of the steel shells. For $T_{\text{shell}} = 293$ K (samples 1 and 2), no bonding between the cast iron and the shell was achieved. In the adjacent cast iron area, cementite needles formed and graphite is present in the form of irregular spheres. Moreover, the matrix of the cast iron core solely comprised pearlite, as expected for the chosen

¹ Hardness values for cast iron depend on the wall thickness of the casting and the production process parameters (DIN EN 1561:2012-01).

(a) Sample 1 (S235JR, 293 K)



(b) Sample 3 (S235JR, 383 K)



(c) Sample 5 (S235JR, 583 K)

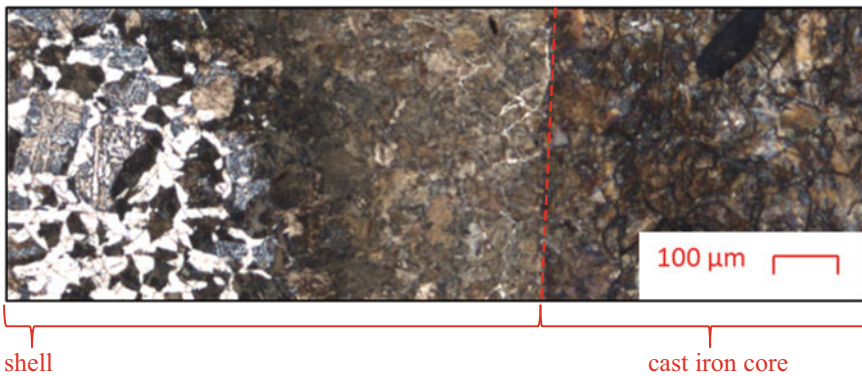
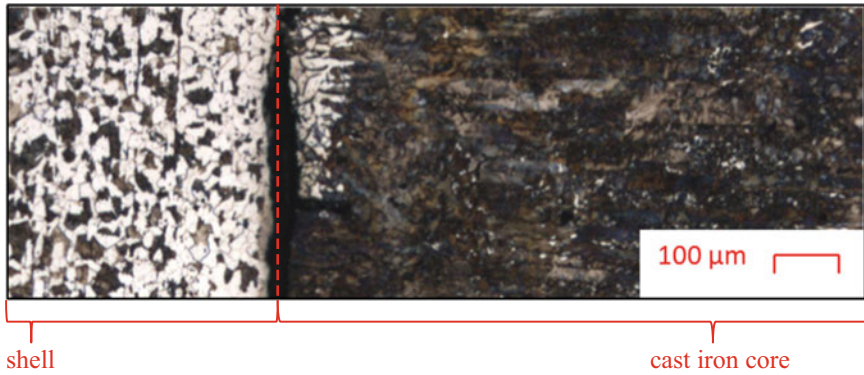
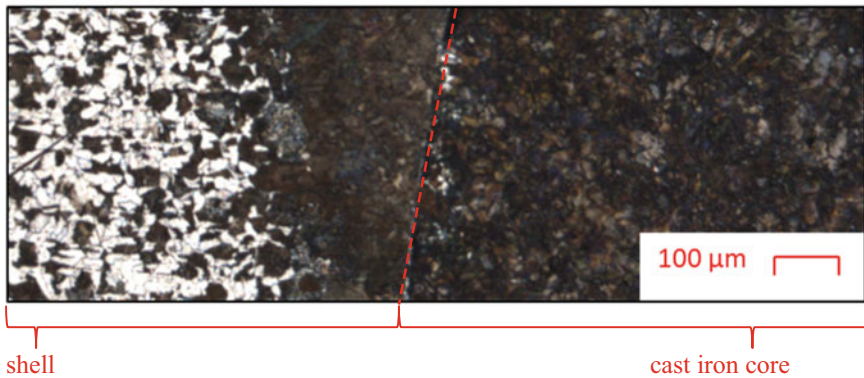


Fig. 14.6 Sections of the etched samples with nomenclature according to Table 14.2, showing the microstructure in the fusion zone for the shell temperatures at the time of the pouring. **a** 293 K, **b** 383 K, **c** 583 K. The shell material S235JR is seen on the left, the EN-GJL-250 cast iron core on the right. The red line indicates the fusion layer

(a) Sample 2 (25CrMo4, 293 K)



(b) Sample 4 (25CrMo4, 383 K)



(c) Sample 6 (25CrMo4, 583 K)

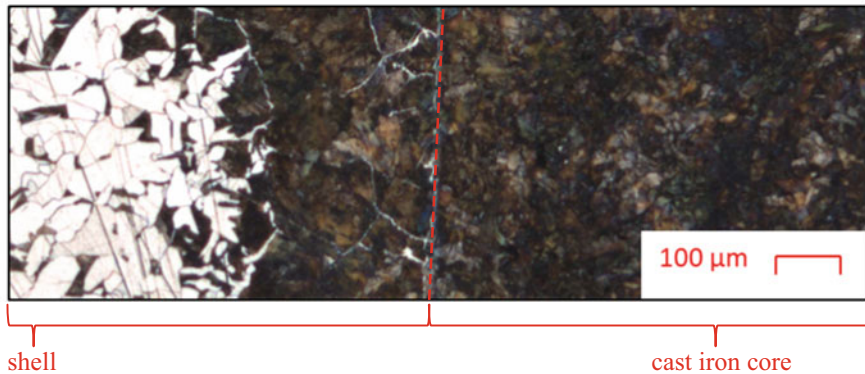


Fig. 14.7 Sections of the etched samples with nomenclature according to Table 14.2, showing the microstructure in the fusion zone for the shell temperatures at the time of the pouring. **a** 293 K, **b** 383 K, **c** 583 K. The shell material 25CrMo4 is seen on the left, the EN-GJL-250 cast iron core on the right. The red line indicates the fusion layer

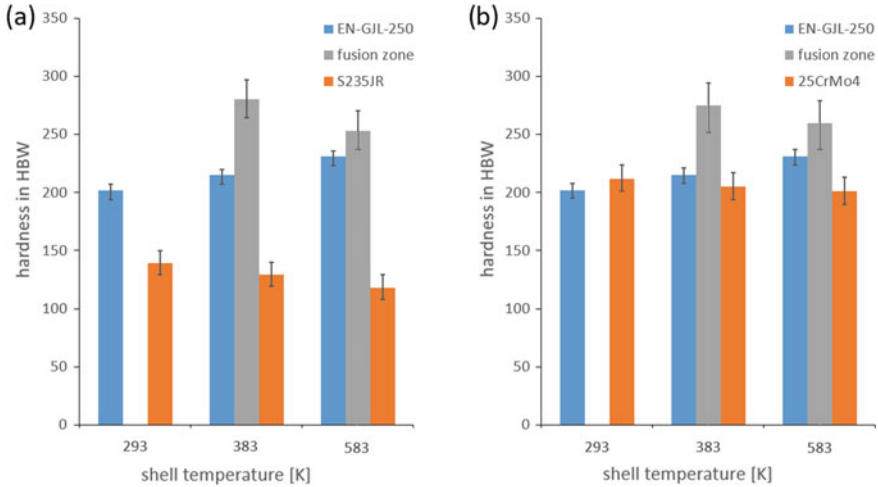


Fig. 14.8 Hardness results for samples created at different preheating temperatures and shell materials **a** shell material S235JR, **b** shell material 25CrMo4

experimental setup (detailed in Sect. 14.2.1). Therefore, the shell likely acted as a chill and increased the cooling rate to such an extent, that it outweighed the graphitization potential of the melt and the influence of inoculation on the formation of stable graphite morphologies. Ferrite seams were present in sample 2. Their formation was promoted by the presence of D-graphite, which provided short diffusion paths for carbon (Elliott 1988; Berns and Theisen 2008). Another possible explanation could be the transition of carbon into the gap between the two materials under the formation of carbon-oxides. This assumption is supported by the fact that the steel shell in this area also becomes decarburized.

Increasing T_{shell} to 383 K (samples 3 and 4) resulted in a non-continuous material-bond connection between the steel shell and the cast iron core. The matrix of the cast iron core was fully pearlitic, and the steel shell underwent a pearlitic transformation up to a depth of 300 μm . The graphite morphology in the fusion zone mainly consisted of supercooled graphite of form D. Only individual graphite lamellae of form A were visible in sample 3, whilst in sample 4 this graphite morphology could be observed locally in the fusion zone. This is somewhat unexpected, as one would correlate the formation of graphite lamellae with a lower cooling rate in this area, whilst the formation of the supercooled graphite further into the cast iron core indicates a high cooling rate. One reason could be the imperfect formation of the fusion zone, where the cooling rate was initially quite low. This could allow for the solidification of a thin cast iron layer with lamellar graphite. After solidification of these fringe areas, they could act as a heat bridge and increase the supercooling of the subsequent areas. D-graphite forms when the cooling rate favours metastable solidification, but this is counteracted by a sufficiently high Si concentration. Although the increase in T_{shell} led to the formation of a diffusion layer, the presence of undesired D-graphite

is an indication for an insufficient shell temperature to ensure the desired graphite morphology (Elliott 1988; Berns and Theisen 2008).

For $T_{\text{shell}} = 583 \text{ K}$ (samples 5 and 6), a continuous fusion zone with a pearlitic matrix was achieved. Pearlinitisation of the steel shell occurred and reached $500 \mu\text{m}$ into the shell, whilst the cast iron core was fully pearlitic. The predominant graphite shape was assigned to form A, with a lesser amount of form E. This was consistent with the typical graphite morphology for EN-GJL-250, although the percentage of IA-graphite is slightly higher in an ideal EN-GJL-250 microstructure (Elliott 1988; Berns and Theisen 2008).

The lack of a fusion zone at 293 K for both shell materials seems to be due to the chilling effect of the steel insert on the solidification of the cast iron melt. At $T_{\text{shell}} = 583 \text{ K}$, the increase in hardness in comparison with the cast iron core can be attributed to either a fine pearlitic microstructure and/or to cementite present in this layer due to the chill effect of the steel shell. A shell temperature of 583 K only led to a minor increase in hardness compared to the cast iron core. The reason is the reduced chilling effect of the steel shell due to the increased temperature of the contact surface, leading to a coarser pearlitic microstructure compared to samples 3 and 4 (Elliott 1988; Berns and Theisen 2008).

An influence of the shell material (S235JR or 25CrMo4) on the fusion zone was not detected, even though the shell materials differed by about 60 HBW in hardness and also in their thermal conductivity. However, both shell materials are rather similar and both belong to the category of low carbon steels. Therefore, it can be concluded that the difference in thermal conductivity of the steels employed as shell materials does not alter the formation of the bonding zone and its properties.

No breakthrough of the melt through the shell was detected. Thus, even with a shell temperature of 583 K at the time of pouring, the local superheating during casting did not result in a leakage of the shell.

14.5 Conclusion

Low carbon steel shells were filled with lamellar graphite cast iron, and the occurring fusion zone was examined. The quality of this zone significantly depends on the temperature of the contact surface between the steel shell and the cast iron melt at the time of pouring. Insufficient preheating of the shell either leads to no material bonding or to undesired microstructural constituents in the area adjacent to the bonding line, such as needle-shaped cementite or ferrite seams. For the setup used in this study, the selected shell temperature of 583 K was sufficient to create a fusion zone that solely consists of pearlite in both the steel shell and the cast iron core. At this temperature, the depth of the fully pearlitic layer extended up to $500 \mu\text{m}$ into the steel shell. It can, therefore, be concluded that a solid bonding between low carbon steel and cast iron can be achieved without the need for any extensive surface treatments, like metallic coatings. The quality of the fusion zone depends almost entirely on the temperature of the contact surface between the shell and the melt. The chemical composition of

the steel shell had no dominant influence on the fusion zone. However, it should be mentioned that for this study only two similar steels were used with a simple geometry and the melt-to-shell ratio was kept constant at 20:1. In an industrial scenario, there are further influencing factors on the microstructure and the properties of the fusion zone in composite casting. These include, but are not limited to, the pouring temperature and chemical composition of the melt and the heat transfer through the mould.

Acknowledgements This project is supported by the Federal Ministry for Economic Affairs and Climate Action (BMWK) on the basis of a decision by the German Bundestag.

References

- Bakke et al (2022) Sn-aided joining of cast aluminum and steel through a compound casting process. *Metall Mater Trans B* 53:60–70
- Berns H, Theisen W (2008) *Eisenwerkstoffe—Stahl und Gusseisen*, 8th edn. Springer, Berlin, pp 31–35
- Buchmayr B, Weligoschek T (2010) Untersuchungen zum Verbundgießen warmfester Legierungen. *Berg Huettenmann Monatsh* 155:318–324
- DIN 50600:2017-10 (2017) *Prüfung metallischer Werkstoffe—Metallographische Gefügebilder—Abbildungsmaßstäbe*. Beuth, Berlin
- DIN 8593:2003 (2003) *Fertigungsverfahren Fügen*. Beuth, Berlin
- DIN EN 1561:2012-01 (2012) *Gießereiwesen—Gusseisen mit Lamellengraphit*. Beuth, Berlin
- DIN EN ISO 6506-1:2014 (2014) *Metallische Werkstoffe—Härteprüfung nach Brinell—Teil 1: Prüfverfahren*. Beuth, Berlin
- DIN EN ISO 945-1:2019 (2019) *Mikrostruktur von Gusseisen—Teil 1: Graphitklassifizierung durch visuelle Auswertung*. Beuth, Berlin
- Dörr J, Wibbeke M (2008) Publication number DE 10 2008 020467 A1. Deutsches Patent- und Markenamt, Bochum
- Elliott (1988) *Cast iron technology*. Butterworth & Co. Ltd, London, pp 1–4, 11–12, 104–105
- Ißleib et al (1995) *Verbundgießen von Eisen-Kohlenstoff-Legierungen—grundlegende metallurgische Reaktionen an der Grenzfläche—Teil I. Gießerei-Praxis* 15(16):286–289
- Jaromin et al (2019) Influence of type and shape of the chill on solidification process of steel casting. *Arch Foundry Eng* 1:35–40
- Khreibtov (2011) *Neuartiges Verfahren zur Online—Prozessüberwachung und—Fehlerklassifizierung beim Durchsetzfügeverbinden von Blechen*. Doctoral thesis, Technical University Clausthal-Zellerfeld
- Krause (1990) *Verbundgießverfahren zur Herstellung spezieller Gussstücke aus Eisenwerkstoffen*. *Gießerei-Praxis* 17:279–282
- Moro (2022) *Fügen durch Stoffvereinigen*. In: *Baukonstruktion—vom Prinzip zum Detail*. Springer, Berlin, pp 314–319
- Noguchi (2008) Trends of composite casting technology and joining technology for castings in Japan. *Int J Cast Met Res* 21:219–225
- Schittenhelm (2018) *Topologieoptimierter Verbund von Aluminium und Stahl zur lokalen Steifigkeitserhöhung von Druckgussbauteilen*. Doctoral thesis, University Bremen
- Technical data sheet 25CrMo4 according to EN 10083-3. Deutsche Edelstahlwerke, Witten (2011)
- Technical data sheet S235JR according to EN 10025-2: 2004. Gruppo Lucefin, Esine (2012)